Yang *et al. Chin. J. Mech. Eng.* (2018) 31:110
https://doi.org/10.1186/s10033-018-0307-5

Chinese Journal of Mechanical Engineering

ORIGINAL ARTICLE

Open Access

Adaptive Backstepping Terminal Sliding Mode Control Method Based on Recurrent Neural Networks for Autonomous Underwater Vehicle

Chao Yang*, Feng Yao and Ming-Jun Zhang

Abstract

The trajectory tracking control problem is addressed for autonomous underwater vehicle (AUV) in marine environment, with presence of the influence of the uncertain factors including ocean current disturbance, dynamic modeling uncertainty, and thrust model errors. To improve the trajectory tracking accuracy of AUV, an adaptive backstepping terminal sliding mode control based on recurrent neural networks (RNN) is proposed. Firstly, considering the inaccurate of thrust model of thruster, a Taylor's polynomial is used to obtain the thrust model errors. And then, the dynamic modeling uncertainty and thrust model errors are combined into the system model uncertainty (SMU) of AUV; through the RNN, the SMU and ocean current disturbance are classified, approximated online. Finally, the weights of RNN and other control parameters are adjusted online based on the backstepping terminal sliding mode controller. In addition, a chattering-reduction method is proposed based on sigmoid function. In chattering-reduction method, the sigmoid function is used to realize the continuity of the sliding mode switching function, and the sliding mode switching gain is adjusted online based on the exponential form of the sliding mode function. Based on the Lyapunov theory and Barbalat's lemma, it is theoretically proved that the AUV trajectory tracking error can quickly converge to zero in the finite time. This research proposes a trajectory tracking control method of AUV, which can effectively achieve high-precision trajectory tracking control of AUV under the influence of the uncertain factors. The feasibility and effectiveness of the proposed method is demonstrated with trajectory tracking simulations and pool-experiments of AUV.

Keywords: Autonomous underwater vehicle (AUV), Trajectory tracking, Neural networks, Backstepping method, Terminal sliding mode, Adaptive control

1 Introduction

Autonomous underwater vehicle (AUV) is widely used to accomplish the assigned tasks in complex marine environment, and also the trajectory tracking control of AUV is one of the important contents of AUV tasks [1]. In complex marine environment, ocean current disturbance [2], dynamic modeling uncertainty (since the hydrodynamic parameters are difficult to measure accurately [3]) and other factors can directly affect the trajectory tracking control accuracy of AUV. Therefore, it has great research significance and practical value to develop the trajectory tracking control method of AUV in marine environment.

Generally, aiming at the problem of AUV trajectory tracking caused by the uncertain factors of ocean current disturbance and dynamic modeling uncertainty, some adaptive control algorithms for trajectory tracking of AUV have been proposed, such as fuzzy adaptive control [4, 5], neural network adaptive control [6–9], which overcome the relevant trajectory tracking control problems to some certain extent. Among them, in Refs. [4, 5], the fuzzy control is used to estimate the uncertain

*Correspondence: yangchao@hrbeu.edu.cn
College of Mechanical and Electrical Engineering, Harbin Engineering University, Harbin 150001, China

factors, but the acquisition of fuzzy rules depends on the knowledge of the designers. Ref. [6] provides a neural network direct adaptive control method, and this method is applied to the control of AUV with bounded external disturbances and bounded neural network approximation errors, and verified by dynamic positioning and single degree of freedom (DOF) trajectory tracking. In Ref. [8], the ocean current disturbances and AUV dynamic modeling uncertainty are considered as uncertainties, the above two uncertainties are combined; then the radial basis function (RBF) neural network is used to approximate the uncertainties online, and the adaptive sliding mode control is adopted to control the AUV. However, in Refs. [6–9], the forward neural network (such as RBF or BP neural network) is difficult to reflect the time series influence of system input and output variables. Therefore, when the target trajectory of AUV has an abrupt change, the neural network weights may take a long time to convergence, leading to poor transition characteristics in trajectory mutation process, and may result in the overshoot of trajectory tracking.

In the actual underwater operations, the motion control of each DOF of AUV is controlled by the control voltage signals, as the control input of thrusters. Due to the complex nonlinear mapping relation between the control voltage, thrust and the velocity of AUV, it is difficult to get the accurate thruster modeling by the typical thrust model identification method [10, 11], it means that there are thrust model errors in thruster model. In the practical control process of AUV, ignoring thrust model errors will lead to the decline of trajectory tracking control accuracy. Based on the above analysis, the thrust model errors factors will be added into the AUV control to improve the trajectory tracking accuracy of AUV.

For the above considerations, in this paper, under the influence of uncertain factors including ocean current disturbance, dynamic modeling uncertainty, and thrust model errors, an adaptive backstepping terminal sliding mode control method based on RNN is proposed for trajectory tracking of AUV. The basic idea of the proposed method is given as follow. Firstly, the thrust model errors are added to the uncertain factors, compared with the methods in Refs. [6, 8, 12, 13] which do not take the thrust model errors into account. And then, due to better transition characteristic and nonlinear identification ability of RNN [14, 15], the SMU and ocean current disturbance (two types of uncertain factors) are classified, approximated online; and the outputs of RNN are used in sliding mode controller. Finally, through the adaptive backstepping terminal controller, the weights of RNN and the control parameters are adjusted online.

Based on the Lyapunov theory and Barbalat's lemma, it is demonstrated that the proposed method can ensure that the tracking error converges to zero in finite time. The trajectory tracking method of AUV combined with neural network and sliding mode control is a typical and commonly used method, as shown in Ref. [8]. Then, based on simulations and pool-experiments, compared with the method in Ref. [8], the feasibility and effectiveness of the proposed method are verified in this paper.

In addition, due to the neural network has approximation errors, the authors and the previous researchers [16, 17] have used neural network and sliding mode control mode to ensure the asymptotic stability of the closed-loop system, but it will introduce the sliding mode chattering problem in AUV control. The chattering problem will lead to the high frequency, high amplitude beating of controller output and affected the trajectory tracking accuracy. Aiming at the chattering problem, a chattering-reduction method is proposed by using sigmoid function instead of discontinuous sliding mode switching term in sliding control. And in the proposed method, the sliding mode switching gain is adjusted online based on the exponential form of sliding mode function. Compared with boundary layer method [18], the simulations are carried out to verify the effectiveness of the proposed method.

This paper is organized as follows. In Section 2, under the influence of the uncertain factors, an adaptive backstepping terminal sliding mode control based on RNN is proposed. Section 3, the stability of the proposed method is analyzed based on Lyapunov theory and Barbalat's lemma. The chattering-reduction method of AUV control variable is presented and analyzed in Section 4. In Section 5, the simulations and pool-experiments of AUV are presented. Finally, conclusions are drawn in Section 6.

2 Control Method Design of AUV

2.1 Basic Ideas of the Method and Problem Statement

To improve the trajectory tracking accuracy of AUV under the influence of the uncertain factors, a trajectory tracking control method of the adaptive backstepping terminal sliding mode based on RNN is proposed. The basic ideas of this method are as follows:

(1) The influence of thrust model errors factors is considered in this method, the thrust model errors are obtained by the Taylor expansion of thruster model. Due to the same nature of thrust model errors and dynamic modeling uncertainty, these two items are combined as the system model uncertainty (in short, SMU) of AUV.
(2) In order to avoid mutual interference of the uncertain factors of SMU and ocean current disturbance, two groups of separate RNN are used to approximate the uncertain factors online, and the RNN outputs are used in the sliding mode controller.

(3) Based on backstepping sliding mode control has a good robustness [13] and the terminal sliding mode can be converged in finite time [19], the backstepping terminal sliding mode is proposed to reduce the convergence time and improve the trajectory tracking accuracy.

To sum up, the control objectives of this paper is to design an adaptive backstepping terminal sliding mode controller u with the target trajectory $[\eta_d, \dot{\eta}_d]^{\mathrm{T}}$ (η, η_{d} are the vectors of actual value and target value of AUV) and make the tracking error z uniformly ultimately bounded, and converges to zero in finite time, under the influence of SMU and ocean current disturbance.

In conclusion, the main process of the proposed method is divided into the following two parts. In Section 2.2, the dynamic model of AUV with thrust model errors is established, and then used two groups of RNN to approximate SMU and ocean current disturbance online. In Section 2.3, an adaptive backstepping terminal sliding mode controller is designed, including the design of the sliding mode surface, sliding mode control law and adaptive control law.

2.2 Dynamic Model of AUV

2.2.1 Typical Dynamic Model in Ocean Environment

The nonlinear dynamic equations of AUV in marine environment can be shown as follows [6, 8, 13, 14]:

$$\begin{aligned}\dot{\eta} = J(\eta)\nu, M\dot{\nu} + C_{RB}(\nu)\nu + C_A(\nu_r)\nu_r \\ + D(\nu_r)\nu_r + g(\eta) + \tau_d = B\tau(u),\end{aligned} \tag{1}$$

where $\eta = [x\ y\ z\ \phi\ \theta\ \psi]^{\mathrm{T}}$ denotes the vector of location and orientation in the earth-fixed frame; $\nu = [u\ v\ w\ p\ q\ r]^{\mathrm{T}}$ is the vector of velocity expressed in the body-fixed frame; M is the inertial matrix, containing the added mass; C_{RB} is the rigid-body Coriolis and Centripetal matrix; C_A is the added mass Coriolis and Centripetal matrix; D is hydrodynamic drag matrix; $g(\eta)$ is the vector of combined gravitational and buoyancy forces; ν_r is the AUV velocity relative to ocean currents ($\nu_r = \nu - \nu_c$, ν_c is ocean currents velocity in body-fixed frame); τ_d is the external disturbance force and the torque vector; $\tau(u)$ is the thruster force and B is the distribution matrix of thrusters; $J(\eta)$ is the transformation matrix between body-fixed frame and earth-fixed frame. The coordinate system definition is shown in Figure 1.

Eq. (1) can be described in the earth-fixed frame as follows:

$$\begin{aligned}M_\eta(\eta)\ddot{\eta} + C_{RB\eta}(\eta, \dot{\eta})\dot{\eta} + C_{A\eta}(\eta_r, \dot{\eta}_r)\dot{\eta}_r \\ + D_\eta(\eta_r, \dot{\eta}_r)\dot{\eta}_r + g_\eta(\eta) + \tau_d = J^{-\mathrm{T}}B\tau(u),\end{aligned} \tag{2}$$

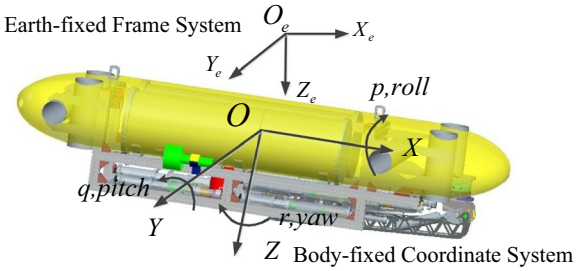

Figure 1 Coordinate system definition

where $M_\eta(\eta) = J^{-\mathrm{T}}MJ^{-1}$; $C_{RB\eta}(\eta, \dot{\eta}) = J^{-\mathrm{T}}(C_{RB}(\nu) - MJ^{-1}\dot{J})J^{-1}$;

$$\begin{aligned}C_{A\eta}(\eta_r, \dot{\eta}_r) &= J^{-\mathrm{T}}C_A(\nu_r)J^{-1}; \\ D(\eta_r, \dot{\eta}_r) &= J^{-\mathrm{T}}D(\nu_r)J^{-1}; \\ g_\eta(\eta) &= J^{-\mathrm{T}}g(\eta).\end{aligned}$$

Based on Refs. [8, 13], dynamic modeling uncertainty is expressed as follows:

$$\begin{aligned}\tilde{M}_\eta = M_\eta - \hat{M}_\eta, \quad \tilde{C}_\eta = C_\eta - \hat{C}_\eta, \\ \tilde{D}_\eta = D_\eta - \hat{D}_\eta, \quad \tilde{g}_\eta = g_\eta - \hat{g}_\eta,\end{aligned} \tag{3}$$

where M_η is real value, $\tilde{M}_\eta$ is estimation value of dynamic modeling established, $\hat{M}_\eta$ is dynamic modeling uncertainty; $C_\eta = C_{RB\eta} + C_{A\eta}$.

Integrating Eqs. (2) and (3), the dynamic model of AUV under ocean current disturbance and dynamic modeling uncertainty can be expressed as:

$$\ddot{\eta} = \hat{M}_\eta^{-1}(J^{-\mathrm{T}}B \cdot \tau(u) - \hat{C}_\eta\dot{\eta} - \hat{D}\dot{\eta} - \hat{g}_\eta) - H, \tag{4}$$

$$\begin{aligned}H = \hat{M}_\eta^{-1}(\tilde{M}_\eta\ddot{\eta} + \tilde{g}_\eta + \tilde{C}_\eta\dot{\eta} + \tilde{D}_\eta\dot{\eta}) \\ + \hat{M}_\eta^{-1}(\tau_d + \overline{C_\eta\eta_r + D_\eta\eta_r}),\end{aligned} \tag{5}$$

where $(\tilde{M}_\eta\ddot{\eta} + \tilde{g}_\eta + \tilde{C}_\eta\dot{\eta} + \tilde{D}_\eta\dot{\eta})$ is the dynamic modeling uncertainty of AUV; and $(\tau_d + \overline{C_\eta\eta_r + D_\eta\eta_r})$ is the ocean current disturbance term, $\tau(u)$ is thruster model.

In Eqs. (4) and (5), it only considered the influence of the ocean current disturbance and the dynamic modeling uncertainty on trajectory tracking. However, in the actual underwater operations, due to the complex nonlinear mapping relation between the control voltage, the thruster thrust and the velocity of AUV, it is difficult to obtain the accurate thruster model $\tau(u)$, based on the typical identification method [10, 11]. And the thrust model errors can directly affect the accuracy of AUV dynamic model, affected the trajectory tracking accuracy of AUV.

Based on the analysis, the dynamic model of AUV with thrust model errors is proposed in Section 2.2.2.

2.2.2 Dynamic Model of AUV with Thrust Model Errors

In this subsection, a mathematical Taylor method is proposed to expand the nonlinear thruster model $\tau(u)$, the specific idea is given as follow. Firstly, through the Taylor expansion of $\tau(u)$, it will get the thrust voltage linear mapping part and thrust model errors part. Then, the thrust voltage linear mapping part will be obtained by the adaptive control law (in Eq. 19); the thrust model errors combined with dynamic modeling uncertainty as the SMU are approximated online, based on RNN.

The steps are summarized as follows.

(1) Taylor Expansion of $\tau(u)$

The thruster model $\tau(u)$ is applied to the Taylor expansion at the control voltage u_i^*. As shown in Eq. (6):

$$\begin{aligned}\tau_i(u_i) &= \lambda_i u_i + \left(\tau_i(u_i^*) - \frac{\partial \tau_i(u_i)}{\partial u_i}\bigg|_{u_i=u_i^*} u_i^* + O\left((u_i - u_i^*)^2\right)\right) \\ &= A(u_i) + B(u_i),\end{aligned} \tag{6}$$

where $A(u_i)$ is thrust voltage linear mapping part; $B(u_i)$ is thrust model errors part (a nonlinear unknown function); $i=1, 2,\ldots, n$ is number of AUV thruster; λ_i is scale factor (unknown positive constant) between voltage and thrust.

Substituting Eq. (6) into Eq. (4), it can be obtained:

$$\begin{aligned}\ddot{\eta} = {} & \hat{M}_\eta^{-1}\left\{J^{-\mathrm{T}} B \cdot [A(u_i) + B(u_i)] - \hat{C}_\eta \dot{\eta} - \hat{D}\dot{\eta} - \hat{g}_\eta\right\} \\ & - \left[\hat{M}_\eta^{-1}(\tilde{M}_\eta \ddot{\eta} + \tilde{\mathrm{g}}_\eta + \tilde{C}_\eta \dot{\eta} + \tilde{D}_\eta \dot{\eta}) \right. \\ & \left. + \hat{M}_\eta^{-1}(\tau_d + \overline{C_\eta \eta_r + D_\eta \eta_r})\right].\end{aligned} \tag{7}$$

Eq. (7) can be rewritten as follows, where $F(\eta)$ and $G(\eta)$ are the SMU and ocean current disturbance, respectively:

$$\begin{aligned}\ddot{\eta} &= \hat{M}_\eta^{-1}\left[J^{-\mathrm{T}} B \cdot A(u_i) - \hat{C}_\eta \dot{\eta} - \hat{D}\dot{\eta} - \hat{g}_\eta\right] - [F(\eta) + G(\eta)], \\ F(\eta) &= \hat{M}_\eta^{-1}\left[\tilde{M}_\eta \ddot{\eta} + \tilde{\mathrm{g}}_\eta + \tilde{C}_\eta \dot{\eta} + \tilde{D}_\eta \dot{\eta} - J^{-\mathrm{T}} B * B(u_i)\right], \\ G(\eta) &= \hat{M}_\eta^{-1}(\tau_d + \overline{C_\eta \eta_r + D_\eta \eta_r}).\end{aligned} \tag{8}$$

Since the $F(\eta)$ and $G(\eta)$ cannot be obtained accurately in practice process, and the $F(\eta)$ and $G(\eta)$ are nonlinear unknown item; therefore, the authors will use neural network to approximate $F(\eta)$, $G(\eta)$ online.

(2) Online Approximation of RNN

In this paper, the RNN can be reflecting the time series influence through the recurrent layer, and it has a better transition characteristic [14, 15]. And also, in order to avoid mutual interference between $F(\eta)$ and $G(\eta)$, two groups of separate RNN is used for online approximation of $F(\eta)$ and $G(\eta)$ (these means the classification, online approximation), and the RNN outputs are used in sliding mode controller.

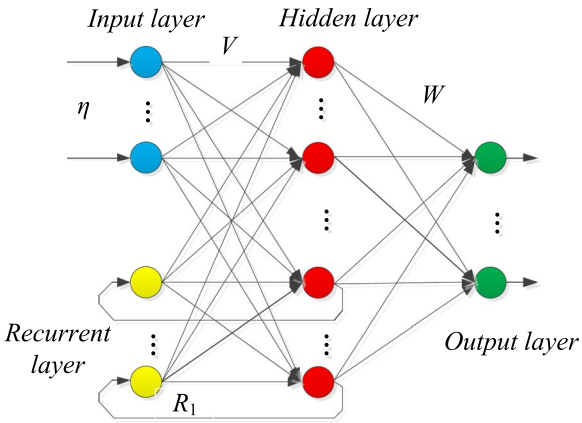

Figure 2 Structure of recurrent neural network

The structure of RNN is shown in Figure 2.

In Figure 2, η ($\eta = [\eta_1, \ldots, \eta_n]^{\mathrm{T}}$) is input layer vector, R_1 ($R_1 = [R_{11}, \ldots, R_{1m}]^{\mathrm{T}}$) is recurrent layer output vector. The output of RNN can be expressed as:

$$f(x) = Wh(VR), \tag{9}$$

where n, m are the numbers of input and recurrent layers, respectively; $h(VR)$ is the output of hidden layer, $R=[\eta, R_1]^{\mathrm{T}}$; W is the network weight matrix between hidden layer and output layer. V is the network weight matrix between input layer, recurrent layer and hidden layer.

According to the nonlinear mapping ability of RNN, there exist the theoretical optimal weight matrices W_F, V_F, W_G, V_G, to make the following equations, such as Eqs. (10a) and (10b), and the $F(\eta)$ and $G(\eta)$ are approximated online by two groups of separate RNN:

$$F(\eta) = W_F h(V_F R_F) + \varepsilon_F, \tag{10a}$$

$$G(\eta) = W_G h(V_G R_G) + \varepsilon_G, \tag{10b}$$

where ε_F, ε_G are approximation errors of RNN, meet $\|\varepsilon_F\| \le \bar{\varepsilon}_F, \|\varepsilon_G\| \le \bar{\varepsilon}_G$, and $\bar{\varepsilon}_F$ and $\bar{\varepsilon}_G$ are positive constant.

Based on the RNN, we will get the estimation value of online approximation as $\hat{F}(\eta)$, $\hat{G}(\eta)$, respectively. The estimated outputs of the RNN are expressed as:

$$\hat{F}(\eta) = \hat{W}_F h\left(\hat{V}_F R_F\right), \tag{11a}$$

$$\hat{G}(\eta) = \hat{W}_G h\left(\hat{V}_G R_G\right), \tag{11b}$$

where $\hat{W}_F$, $\hat{W}_G$, $\hat{V}_F$, $\hat{V}_G$ is estimate value of weight.

2.3 Adaptive Sliding Mode Controller Design

Adaptive sliding mode control, as a typical control method for nonlinear system, has been widely used in nonlinear uncertain systems [20, 21], such as AUV and underwater manipulators. Different from the current researches, such as Refs. [6, 8, 14], a controller was adopted in this paper, by combining with backstepping design and terminal sliding mode theory. Hence, the trajectory tracking error can be quickly converged to zero in finite time and the robustness of AUV control system is improved.

(1) Backstepping Terminal Sliding Surface

To ensure that the sliding mode surface could be quickly converged to zero in finite time, on the basis of non-singular terminal sliding mode [22] and backstepping idea [23], a nonlinear sliding mode surface was constructed, shown in Eq. (12):

$$s = z_1 + kz_2^{p/q} = z_1 + k|z_2|^{p/q}\mathrm{sgn}(z_2), \tag{12}$$

where $k>0$ is positive constant, $1<\gamma=p/q<2$; sliding mode surface $s=[s_1, s_2, \ldots, s_6]^{\mathrm{T}}$.

Based on the backstepping idea, the trajectory tracking error system variables z_1 and z_2 can be rewritten as:

$$\begin{aligned} z_1 &= \eta - \eta_d, \\ z_2 &= \dot{\eta} - \dot{\eta}_d - \alpha, \end{aligned} \tag{13}$$

where $\alpha = -c_1 z_1$, c_1 is positive constant; η, η_d are the vectors of actual value and target value of AUV in the earth-fixed frame, respectively.

Substituting Eq. (8) into the derivative of backstepping terminal sliding surface, and then it can be expressed as:

$$\begin{aligned} \dot{s} = \dot{z}_1 + k\gamma|z_2|^{\gamma-1}\dot{z}_2 &= \dot{z}_1 + k\gamma|z_2|^{\gamma-1} \\ &\times \left[\hat{M}_\eta^{-1}(J^{-\mathrm{T}}B\hat{\lambda}u - \hat{C}_\eta\dot{\eta} - \hat{D}\dot{\eta} - \hat{g}_\eta)\right. \\ &\left.-(F(\eta)+G(\eta)) - \ddot{\eta}_d - \dot{\alpha}\right]. \end{aligned} \tag{14}$$

(2) Sliding Mode Control Laws and Adaptive Laws

Based on the Lyapunov stability theory and nonlinear sliding mode surface in Eq. (12), the main control laws are given as follows.

Consider the AUV dynamic system, described by Eq. (8), and under the control of adaptive backstepping terminal sliding mode controller (sliding mode control laws) based on RNN in Eq. (15), weight adaptive laws of RNN in Eq. (16), and adaptive law of thrust model scale factors in Eq. (17), then all the signals of AUV system are bounded and the AUV trajectory tracking error system could converge to zero in a finite time.

$$\begin{aligned} u = \hat{\lambda}^{-1}J^{\mathrm{T}}B^{-1}[&H + \hat{M}_\eta(\ddot{\eta}_d + \dot{\alpha} + \hat{F}(\eta)+\hat{G}(\eta)) \\ &- \hat{M}_\eta k^{-1}\gamma^{-1}|z_2|^{2-\gamma}\mathrm{sgn}(z_2) \\ &- \hat{M}_\eta k^{-1}\gamma^{-1}|z_2|^{1-\gamma}(hs + \hat{\lambda}\mathrm{sgn}(s))], \end{aligned} \tag{15a}$$

$$H = \hat{C}_\eta\dot{\eta} + \hat{D}\dot{\eta} + \hat{g}_\eta, \tag{15b}$$

$$\dot{\hat{W}}_F = -k_1\Gamma_{WF}\chi\,\mathrm{sh}(\hat{V}_F R_F)^{\mathrm{T}}, \tag{16a}$$

$$\dot{\hat{W}}_G = -k_2\Gamma_{WG}\chi\,\mathrm{sh}(\hat{V}_G R_G)^{\mathrm{T}}, \tag{16b}$$

$$\dot{\hat{V}}_F = -k_3\Gamma_{VF}\left[\hat{W}_F h'(\hat{V}_F R_F)\right]^{\mathrm{T}}\chi s R_F^{\mathrm{T}}, \tag{16c}$$

$$\dot{\hat{V}}_G = -k_4\Gamma_{VG}\left[\hat{W}_G h'(\hat{V}_G R_G)\right]^{\mathrm{T}}\chi s R_G^{\mathrm{T}}, \tag{16d}$$

$$\chi = kr|z_2|^{r-1}, \tag{16e}$$

$$\dot{\hat{\lambda}} = k_5 s^{\mathrm{T}}\mathrm{sgn}(s). \tag{17}$$

where k_i ($i=1,2,\ldots,5$) is positive constant, $\hat{\lambda}$ is estimated value of scale factor λ, h is positive constant.

In order to design and verify the stability and finite time convergence of the backstepping terminal sliding mode control, we need to use the following lemma.

Lemma 1 [24] For the any real number x_i, $i=1,\ldots, n$, and $0<b<1$, the following inequality holds

$$(|x_1|+|x_2|+\cdots+|x_n|)^b \le |x_1|^b + \left|x_2\right|^b + \cdots + |x_n|^b.$$

Lemma 2 [25] Assume that a continuous positive definite function $V(t)$ satisfies the following differential inequality:

$$\dot{V}(t) \le -\tau V^{\theta}(t), \quad \forall t \ge t_0, \quad V(t_0) \ge 0,$$

where $\tau>0$, $0<\theta<1$ are constant. For any t_0, $V(t)$ satisfy the following inequality:

$$\begin{aligned} &V^{1-\theta}(t) \le V^{1-\theta}(t_0) - \tau(1-\theta)(t-t_0), \quad t_0 \le t \le t_1, \\ &V(t) = 0, \quad \forall t \ge t_1. \end{aligned}$$

The convergence time t_1 is described as follows:

$$t_1 = t_0 + \frac{V^{1-\theta}(t_0)}{n(1-\theta)},$$

where $V(t_0)$ is the initial value and t_0 is the initial time.

3 Stability Analysis

Consider the candidate Lyapunov function

$$V = \frac{1}{2}z_1^{\mathrm{T}}z_1 + \frac{1}{2}s^{\mathrm{T}}s + \frac{1}{2k_1}tr\left(\tilde{W}_F^{\mathrm{T}}\Gamma_{WF}^{-1}\tilde{W}_F\right) + \frac{1}{2k_2}tr\left(\tilde{W}_G^{\mathrm{T}}\Gamma_{WG}^{-1}\tilde{W}_G\right) + \frac{1}{2k_3}tr\left(\tilde{V}_F^{\mathrm{T}}\Gamma_{VF}^{-1}\tilde{V}_F\right) + \frac{1}{2k_4}tr\left(\tilde{V}_G^{\mathrm{T}}\Gamma_{VG}^{-1}\tilde{V}_G\right) + \frac{1}{2k_5}\left(\lambda-\hat{\lambda}\right)^2. \tag{18}$$

According to sliding surface Eq. (12) and Eq. (14), the time derivative of Lyapunov function could be obtained as Eq. (19). Substituting Eq. (15) into (19), we can get Eq. (20):

$$\begin{aligned}\dot{V} &= z_1^{\mathrm{T}}\dot{z}_1 + s^{\mathrm{T}}\dot{s} + \frac{1}{k_1}tr\left(\tilde{W}_F^{\mathrm{T}}\Gamma_{WF}^{-1}\dot{\tilde{W}}_F\right) + \frac{1}{k_2}tr\left(\tilde{W}_G^{\mathrm{T}}\Gamma_{WG}^{-1}\dot{\tilde{W}}_G\right) + \frac{1}{k_3}tr\left(\tilde{V}_F^{\mathrm{T}}\Gamma_{VF}^{-1}\dot{\tilde{V}}_F\right) + \frac{1}{k_4}tr\left(\tilde{V}_G^{\mathrm{T}}\Gamma_{VG}^{-1}\dot{\tilde{V}}_G\right) + \frac{1}{k_5}\left(\lambda-\hat{\lambda}\right)\dot{\tilde{\lambda}} \\ &= z_1^{\mathrm{T}}\dot{z}_1 + s^{\mathrm{T}}\dot{z}_1 + s^{\mathrm{T}}k\gamma|z_2|^{\gamma-1}\left[\hat{M}_\eta^{-1}(J^{-\mathrm{T}}B\hat{\lambda}u - \hat{C}_\eta\dot{\eta} - \hat{D}\dot{\eta} - \hat{g}_\eta) - (F(\eta)+G(\eta)) - \ddot{\eta}_d - \dot{\alpha}\right] + \frac{1}{k_1}tr\left(\tilde{W}_F^{\mathrm{T}}\Gamma_{WF}^{-1}\dot{\tilde{W}}_F\right) \\ &\quad + \frac{1}{k_2}tr\left(\tilde{W}_G^{\mathrm{T}}\Gamma_{WG}^{-1}\dot{\tilde{W}}_G\right) + \frac{1}{k_3}tr\left(\tilde{V}_F^{\mathrm{T}}\Gamma_{VF}^{-1}\dot{\tilde{V}}_F\right) + \frac{1}{k_4}tr\left(\tilde{V}_G^{\mathrm{T}}\Gamma_{VG}^{-1}\dot{\tilde{V}}_G\right) - \frac{1}{k_5}\left(\lambda-\hat{\lambda}\right)\dot{\tilde{\lambda}},\end{aligned} \tag{19}$$

$$\begin{aligned}\dot{V} &= z_1^{\mathrm{T}}(-c_1z_1 + z_2) - c_1z_1^{\mathrm{T}}s - s^{\mathrm{T}}k\gamma|z_2|^{\gamma-1} \times \left[(F(\eta)-\hat{F}(\eta))+(G(\eta)-\hat{G}(\eta))\right] - s^{\mathrm{T}}hs - s^{\mathrm{T}}\hat{\lambda}\mathrm{sgn}(s) \\ &\quad + \frac{1}{k_1}tr\left(\tilde{W}_F^{\mathrm{T}}\Gamma_{WF}^{-1}\dot{\tilde{W}}_F\right) + \frac{1}{k_2}tr\left(\tilde{W}_G^{\mathrm{T}}\Gamma_{WG}^{-1}\dot{\tilde{W}}_G\right) + \frac{1}{k_3}tr\left(\tilde{V}_F^{\mathrm{T}}\Gamma_{VF}^{-1}\dot{\tilde{V}}_F\right) + \frac{1}{k_4}tr\left(\tilde{V}_G^{\mathrm{T}}\Gamma_{VG}^{-1}\dot{\tilde{V}}_G\right) - \frac{1}{k_5}\left(\lambda-\hat{\lambda}\right)\dot{\tilde{\lambda}}.\end{aligned} \tag{20}$$

where $z_2 = |z_2|\mathrm{sgn}(z_2)$, $s^{\mathrm{T}}c_1z_1 = c_1z_1^{\mathrm{T}}s$.

Due to

$$\begin{aligned}&z_1^{\mathrm{T}}(-c_1z_1 + z_2) - c_1z_1^{\mathrm{T}}s = -c_1z_1^{\mathrm{T}}z_1 + z_1^{\mathrm{T}}z_2 - c_1z_1^{\mathrm{T}}(z_1 + k|z_2|^{\gamma}\mathrm{sgn}(z_2)) \\ &= -2c_1z_1^{\mathrm{T}}z_1 + z_2^{\mathrm{T}}z_1 - c_1k|z_2|^{\gamma-1}z_1^{\mathrm{T}}z_2.\end{aligned} \tag{21}$$

The positive definite matrix $\boldsymbol{Q}$ which is constructed in this paper is shown by the following Eq. (22):

$$\boldsymbol{Q} = \begin{bmatrix} \mathrm{diag}(2c_1, 2c_1, 2c_1) & \mathrm{diag}(c_1k|z_2|^{\gamma-1}) \\ -I_{3\times3} & O_{3\times3} \end{bmatrix}. \tag{22}$$

In Eq. (22), $\|Q\| = c_1\left\|k|z_2|^{\gamma-1}\right\| \geq 0$, $\boldsymbol{I}_{3\times3}$ and $\boldsymbol{O}_{3\times3}$ are third order identity matrix and third order null matrix, respectively. Then, Eq. (21) can be expressed by the positive definite matrix $\boldsymbol{Q}$ as follows:

$$\begin{aligned}&z_1^{\mathrm{T}}(-c_1z_1 + z_2) - c_1z_1^{\mathrm{T}}s \\ &= -2c_1z_1^{\mathrm{T}}z_1 + z_2^{\mathrm{T}}z_1 - c_1k|z_2|^{\gamma-1}z_1^{\mathrm{T}}z_2 \\ &= -\begin{bmatrix} z_1^{\mathrm{T}} & z_2^{\mathrm{T}} \end{bmatrix}\boldsymbol{Q}\begin{bmatrix} z_1 \\ z_2 \end{bmatrix}.\end{aligned} \tag{23}$$

According to Eq. (23), Eq. (20) can be converted to

$$\begin{aligned}\dot{V} &= -\begin{bmatrix} z_1^{\mathrm{T}} & z_2^{\mathrm{T}} \end{bmatrix}Q\begin{bmatrix} z_1 \\ z_2 \end{bmatrix} - s^{\mathrm{T}}k\gamma|z_2|^{\gamma-1} \times \left[(F(\eta)-\hat{F}(\eta))+(G(\eta)-\hat{G}(\eta))\right] - s^{\mathrm{T}}hs - s^{\mathrm{T}}\hat{\lambda}\mathrm{sgn}(s) + \frac{1}{k_1}tr\left(\tilde{W}_F^{\mathrm{T}}\Gamma_{WF}^{-1}\dot{\tilde{W}}_F\right) \\ &\quad + \frac{1}{k_2}tr\left(\tilde{W}_G^{\mathrm{T}}\Gamma_{WG}^{-1}\dot{\tilde{W}}_G\right) + \frac{1}{k_3}tr\left(\tilde{V}_F^{\mathrm{T}}\Gamma_{VF}^{-1}\dot{\tilde{V}}_F\right) + \frac{1}{k_4}tr\left(\tilde{V}_G^{\mathrm{T}}\Gamma_{VG}^{-1}\dot{\tilde{V}}_G\right) - \frac{1}{k_5}\left(\lambda-\hat{\lambda}\right)\dot{\tilde{\lambda}}.\end{aligned} \tag{24}$$

Among them, the uncertain factors $F(\eta)$ and $G(\eta)$ are the online approximation term of RNN, the approximation error is given as follows:

$$\begin{aligned}&\left(F(\eta)-\hat{F}(\eta)\right) + \left(G(\eta)-\hat{G}(\eta)\right) \\ &= \left(W_Fh(V_FR_F) - \hat{W}_Fh\left(\hat{V}_FR_F\right)\right) + \left(W_Gh(V_GR_G) - \hat{W}_Gh\left(\hat{V}_GR_G\right)\right) + (\varepsilon_F + \varepsilon_G).\end{aligned} \tag{25}$$

Then, the Taylor expansion of $h(V_FR_F)$, $h(V_GR_G)$ about $\hat{V}_FR_F$, $\hat{V}_GR_G$, respectively:

$$\begin{aligned}h(V_FR_F) &= h\left(\hat{V}_FR_F\right) + \left.\frac{\partial h(V_FR_F)}{\partial\hat{V}_FR_F}\right|_{V_FR_F=\hat{V}_FR_F}\left(V_FR_F - \hat{V}_FR_F\right) + o\left(\left(V_FR_F - \hat{V}_FR_F\right)^2\right), \\ h(V_GR_G) &= h\left(\hat{V}_GR_G\right) + \left.\frac{\partial h(V_GR_G)}{\partial\hat{V}_GR_G}\right|_{V_GR_G=\hat{V}_GR_G}\left(V_GR_G - \hat{V}_GR_G\right) + o\left(\left(V_GR_G - \hat{V}_GR_G\right)^2\right).\end{aligned} \tag{26}$$

Substituting Eq. (26) into (25):

$$\begin{aligned}&\left(F(\eta)-\hat{F}(\eta)\right) + \left(G(\eta)-\hat{G}(\eta)\right) \\ &= \tilde{W}_Fh\left(\hat{V}_FR_F\right) + \hat{W}_Fh'\left(\hat{V}_FR_F\right)\tilde{V}_FR_F + \tilde{W}_Gh\left(\hat{V}_GR_G\right) + \hat{W}_Gh'\left(\hat{V}_GR_G\right)\tilde{V}_GR_G + w_1 + w_2,\end{aligned} \tag{27}$$

where $\tilde{W}_G = W_G - \hat{W}_G, \tilde{V}_G = V_G - \hat{V}_G, \tilde{W}_F = W_F - \hat{W}_F, \tilde{V}_F = V_F - \hat{V}_F$ are weight estimation errors. And the uncertain term w_1, w_2 after Taylor expansion are shown in Eq. (28):

$$\begin{aligned} w_1 &= \tilde{W}_F h'\left(\hat{V}_F R_F\right)\tilde{V}_F R_F + W_F O\left(\tilde{V}_F R_F\right)^2 + \varepsilon_F, \\ w_2 &= \tilde{W}_G h'\left(\hat{V}_G R_G\right)\tilde{V}_G R_G + W_G O\left(\tilde{V}_G R_G\right)^2 + \varepsilon_G. \end{aligned} \tag{28}$$

Through Eqs. (15), (16) and (17), it can be obtained

$$\begin{aligned} \dot{V} = &- \begin{bmatrix} z_1^{\mathrm{T}} & z_2^{\mathrm{T}} \end{bmatrix} Q \begin{bmatrix} z_1 \\ z_2 \end{bmatrix} - s^{\mathrm{T}} \chi \Big[\tilde{W}_F h\left(\hat{V}_F R_F\right) \\ &+ \tilde{W}_G h\left(\hat{V}_G R_G\right) \\ &+ \hat{W}_F h'\left(\hat{V}_F R_F\right)\tilde{V}_F R_F + \hat{W}_G h'\left(\hat{V}_G R_G\right)\tilde{V}_G R_G \Big] \\ &- \frac{1}{k_1} tr\left(\tilde{W}_F^{\mathrm{T}} \Gamma_{WF}^{-1} \dot{\hat{W}}_F\right) - \frac{1}{k_2} tr\left(\tilde{W}_G^{\mathrm{T}} \Gamma_{WG}^{-1} \dot{\hat{W}}_G\right) \\ &- \frac{1}{k_3} tr\left(\tilde{V}_F^{\mathrm{T}} \Gamma_{VF}^{-1} \dot{\hat{V}}_F\right) - \frac{1}{k_4} tr\left(\tilde{V}_G^{\mathrm{T}} \Gamma_{VG}^{-1} \dot{\hat{V}}_G\right) \\ &- s^{\mathrm{T}} hs - s^{\mathrm{T}} \lambda \mathrm{sgn}(s) - s^{\mathrm{T}} \chi (w_1 + w_2) \\ &+ \tilde{\lambda}\left(s^{\mathrm{T}} \mathrm{sgn}(s) - \frac{1}{k_5}\dot{\hat{\lambda}}\right) \le - \begin{bmatrix} z_1^{\mathrm{T}} & z_2^{\mathrm{T}} \end{bmatrix} Q \begin{bmatrix} z_1 \\ z_2 \end{bmatrix} \\ &- s^{\mathrm{T}} hs + \|s\|(\|\chi (w_1 + w_2)\| - \lambda). \end{aligned} \tag{29}$$

Due to $\|\varepsilon_F\| \le \bar{\varepsilon}_F, \|\varepsilon_G\| \le \bar{\varepsilon}_G$ bounded, and the remaining items in Eq. (28) are very small, hence the values of w_1, w_2 in Eq. (28) would be bounded. Assuming that there exists an unknown positive constant λ (the scale factor in Eq. (6) which is adjusted online by the adaptive controller) to ensure w_1, w_2 to satisfy the following equation:

$$\|\chi (w_1 + w_2)\| \le \|\chi w_1\| + \|\chi w_2\| \le \chi (\bar{\varepsilon}_F + \bar{\varepsilon}_G) \le \lambda, \tag{30}$$

where $\|\cdot\|$ denotes Euclidean norm.

According to Eq. (30), Eq. (29) can be simplified as

$$\dot{V} \le - \begin{bmatrix} z_1^{\mathrm{T}} & z_2^{\mathrm{T}} \end{bmatrix} Q \begin{bmatrix} z_1 \\ z_2 \end{bmatrix}. \tag{31}$$

Through Eq. (31), it can be proving that $\dot{V} \le 0$.

According to the Lyapunov theory and Eq. (31), the tracking error z_1, sliding mode surface s, neural network weight $\tilde{W}_F$, $\tilde{W}_G$, $\tilde{V}_F$, $\tilde{V}_G$ and scale factor $\tilde{\lambda}$ are bounded. Due to the boundedness of $\dot{\eta}$ and $\dot{\eta}_d$, the parameters of α and z_2 are also bounded.

Next, the authors will prove that the system states in Eq. (12) can reach nonsingular backstepping terminal sliding surface $s = 0$ within a finite time.

Due to the boundedness of $\tilde{\lambda}$, assume that there is a positive constants λ^*, satisfies the inequality $\hat{\lambda} \le \lambda^*$ for any $t \ge 0$. Similar to the Ref. [20], the following Lyapunov function is used to analyze whether the system states can converge to zero in finite time:

$$V_1 = \frac{1}{2} z_1^{\mathrm{T}} z_1 + \frac{1}{2} s^{\mathrm{T}} s + \frac{1}{2r_0}\left(\lambda^* - \hat{\lambda}\right)^2, \tag{32}$$

where r_0 is a known positive constant.

The time derivative of Eq. (32), substituting Eq. (23) into (32):

$$\begin{aligned} \dot{V}_1 = &- \begin{bmatrix} z_1^{\mathrm{T}} & z_2^{\mathrm{T}} \end{bmatrix} Q \begin{bmatrix} z_1 \\ z_2 \end{bmatrix} - s^{\mathrm{T}} k\gamma |z_2|^{\gamma - 1} \\ &\times \left[\left(F(\eta) - \hat{F}(\eta)\right) + \left(G(\eta) - \hat{G}(\eta)\right)\right] \\ &- s^{\mathrm{T}}(hs + \hat{\lambda}\mathrm{sgn}(s)) - \frac{1}{r_0}\left(\lambda^* - \hat{\lambda}\right)\dot{\hat{\lambda}}. \end{aligned} \tag{33}$$

According to the above analysis, the $\tilde{W}_F$, $\tilde{W}_G$, $\tilde{V}_F$, $\tilde{V}_G$of RNN and w_1, w_2 are bounded. Therefore, $\tilde{W}_F h\left(\hat{V}_F R_F\right)$, $\tilde{W}_G h\left(\hat{V}_G R_G\right)$, $\hat{W}_F h'\left(\hat{V}_F R_F\right)\tilde{V}_F R$, $\hat{W}_G h'\left(\hat{V}_G R_G\right)\tilde{V}_G R_G$ are bounded. Then, based on Eq. (27), the approximation error of system uncertainty item $\left(F(\eta) - \hat{F}(\eta)\right) + \left(G(\eta) - \hat{G}(\eta)\right)$ is bounded. Hence, there exists a positive definite matrix $N = \mathrm{diag}(N_1, N_2, \ldots, N_n)$ for $N_n \ge 0$ satisfies the following equations:

$$\begin{aligned} &\tilde{W}_F h\left(\hat{V}_F R_F\right) + \hat{W}_F h'\left(\hat{V}_F R_F\right)\tilde{V}_F R_F + \tilde{W}_G h\left(\hat{V}_G R_G\right) \\ &+ \hat{W}_G h'\left(\hat{V}_G R_G\right)\tilde{V}_G R_G + w_1 + w_2 \le N. \end{aligned}$$

Consequently, it can be obtained:

$$\begin{aligned} \dot{V}_1 &= - \begin{bmatrix} z_1^{\mathrm{T}} & z_2^{\mathrm{T}} \end{bmatrix} \boldsymbol{Q} \begin{bmatrix} z_1 \\ z_2 \end{bmatrix} - s^{\mathrm{T}} k\gamma |z_2|^{\gamma - 1} N - s^{\mathrm{T}} hs \\ &\quad - \hat{\lambda}\mathrm{sgn}(s) - \frac{1}{r_0}\left(\lambda^* - \hat{\lambda}\right)\dot{\hat{\lambda}} \\ &\le - \begin{bmatrix} z_1^{\mathrm{T}} & z_2^{\mathrm{T}} \end{bmatrix} \boldsymbol{Q} \begin{bmatrix} z_1 \\ z_2 \end{bmatrix} \\ &\quad - (k\gamma |z_2|^{\gamma - 1} N + \hat{\lambda})|s| - \frac{1}{r_0}\left(\lambda^* - \hat{\lambda}\right)\dot{\hat{\lambda}}. \end{aligned} \tag{34}$$

Due to $\hat{\lambda} \le \lambda^*$, then substituting Eq. (17) into (34), we can obtain

$$\begin{aligned} \dot{V}_1 &\le - \begin{bmatrix} z_1^{\mathrm{T}} & z_2^{\mathrm{T}} \end{bmatrix} Q \begin{bmatrix} z_1 \\ z_2 \end{bmatrix} \\ &\quad - (k\gamma |z_2|^{\gamma - 1} N + \hat{\lambda})|s| - \frac{k_5}{r_0}|s|\left|\lambda^* - \hat{\lambda}\right| \\ &\le -\tau_z |z_1| - \tau_s |s| - \tau_d \left|\lambda^* - \hat{\lambda}\right|, \end{aligned} \tag{35}$$

Where τ_z satisfies $-\begin{bmatrix} z_1^{\mathrm{T}} & z_2^{\mathrm{T}} \end{bmatrix} Q \begin{bmatrix} z_1 \\ z_2 \end{bmatrix} \leq -\tau_z |z_1|$, τ_s is minimum element of vector $k\gamma |z_2|^{\gamma-1} N + \hat{\lambda}$, and $\tau_d = (k_5 / r_0)|s|$.

The upper inequality can be converted to

$$\begin{aligned} \dot{V}_1 &\leq -\sqrt{2}\tau_z \frac{|z_1|}{\sqrt{2}} - \sqrt{2}\tau_s \frac{|s|}{\sqrt{2}} - \sqrt{2}\tau_d \frac{\left|\lambda^* - \hat{\lambda}\right|}{\sqrt{2}} \\ &\leq -\min\left(\sqrt{2}\tau_z, \sqrt{2}\tau_s, \sqrt{2}\tau_d\right) \left(\frac{|z_1|}{\sqrt{2}} + \frac{|s|}{\sqrt{2}} + \frac{\left|\lambda^* - \hat{\lambda}\right|}{\sqrt{2}} \right). \end{aligned} \tag{36}$$

According to Lemma 1, definition $\tau = \min\left(\sqrt{2}\tau_z, \sqrt{2}\tau_s, \sqrt{2}\tau_d\right)$, it can yield:

$$\dot{V}_1 \leq -\tau \left[\left(\frac{|z_1|}{\sqrt{2}} \right)^2 + \left(\frac{|s|}{\sqrt{2}} \right)^2 + \left(\frac{\left|\lambda^* - \hat{\lambda}\right|}{\sqrt{2}} \right)^2 \right]^{\frac{1}{2}} = -\tau V_1^{\frac{1}{2}}. \tag{37}$$

Then, based on Barbalat's lemma (Lemma 2), AUV tracking error system can converge to zero (it also means sliding surface $s=0$) in a finite time under the control of the proposed method. The specific convergence time is:

$$T = \frac{2V_1^{1/2}(0)}{\tau}. \tag{38}$$

Proof is completed.

4 Chattering-Reduction Method

The sliding mode control can drive system state variables to equilibrium by a discontinuous feedback control law [26]. Aiming at the chattering problem caused by the discontinuous sliding mode switching term, some typical chattering-reduction methods have been proposed, such as adaptive learning method [27, 28], boundary layer method [18, 29], and so on. Among them, the adaptive learning method needs to simultaneously online learning the model uncertainties and sliding mode switching gain, which could affect the convergence speed of neural network online learning, so it is not suitable for the AUV control system in this paper. The boundary layer method replaces the discontinuous switching terms in the traditional sliding mode control by the saturation function to achieve the continuity of sliding mode switching, and then reduces the chattering problem which caused by the discontinuous switching of the sliding mode. Due to the method is simple and effective; the boundary layer method is one of the commonly used methods to reduce the chattering problem, as shown in Refs. [13, 18, 27, 29]. However, in the experimental study of the boundary layer method, it is found that the method can reduce the chattering amplitude of control variable to a certain extent, but the reduction effect of chattering frequency is not effective.

To reduce the chattering phenomenon, a chattering-reduction method of control variables is proposed in this paper. In the method, the discontinuous switching term of sliding mode control is replaced by the combination of sigmoid function and sliding surface s, to realize the continuity of sliding mode switching function. And the sliding mode switch gain is dynamically adjusted online through the exponential function of sliding surface s.

The steps of chattering-reduction method are as follows.

(1) Continuous function of chattering-reduction method

The sigmoid function and sliding surface s are incorporated as follows:

$$\Delta = K_1 s + K_2 |s|^{\rho} \mathrm{sig}(s), \tag{39}$$

where Δ is $K_1 = \mathrm{diag}(K_{11}, \ldots, K_{1n})$, sliding mode switch gain $K_2 = \mathrm{diag}(K_{21}, \ldots, K_{2n})$, $0 < \rho < 1$, $\mathrm{sig}(s)$ is the continuous sigmoid function.

(2) Sliding mode switch gain K_2

For the sliding mode control, when the system has a large tracking error, the K_2 should have a larger value, so as to ensure the quickly convergence. While AUV is close to the target, the K_2 should be decreased to reduce the chattering of the control system. For this purpose, the sliding mode switch gain K_2 is shown as follows:

$$K_2 = \exp\left(|\varepsilon s| - d_1\right), \tag{40}$$

where ε is a positive definite diagonal matrix; d_1 is positive constant.

Substituting Eq. (39) into the control laws Eq. (15), the final control laws of the system are presented as follows:

$$\begin{aligned} u = J^{\mathrm{T}}(B\hat{\lambda})^{-1} [& H + \hat{M}_\eta (\ddot{\eta}_d + \dot{\alpha} + \hat{F}) \\ & - \hat{M}_\eta k^{-1} \gamma^{-1} |z_2|^{2-\gamma} \mathrm{sgn}(z_2) \\ & - \hat{M}_\eta k^{-1} \gamma^{-1} |z_2|^{1-\gamma} (hs + \hat{\lambda}(K_1 s + K_2 |s|^{\rho} \mathrm{sig}(s))], \end{aligned} \tag{41a}$$

$$H = \hat{C}_\eta \dot{\eta} + \hat{D} \dot{\eta} + \hat{g}_\eta. \tag{41b}$$

Based on the above analysis, under the influence of the uncertain factors, an adaptive backstepping terminal sliding mode control based on RNN is proposed, and under the controller of the proposed method (Eq. (41), Eq. (16), Eq. (17)), it can be guaranteed that the tracking error can achieve finite-time stability.

5 Simulations and Pool-Experiments

In order to validate the feasibility and effectiveness of the proposed adaptive backstepping sliding mode control method based on RNN and the proposed chattering-reduction method, serial simulations of ROPOS AUV and pool-experiments of UVIC-I AUV are carried out.

5.1 Simulation Verification

Under the influence of the ocean current disturbance, dynamic modeling uncertainty, and thrust model errors, the tracking performance of the proposed method is verified by comparison with the method in Ref. [8]. And compared with the boundary layer method in Ref. [18], the effectiveness of the proposed chattering-reduction method is verified.

In the simulations, the dynamic model of ROPOS AUV in Ref. [30] is adopted, and the dynamic parameters of the underwater vehicle are shown in Table 1, and there are two horizontal thrusters, two lateral thrusters and four vertical thrusters (abbreviated as T1, T2, T3, T4, T5, T6, T7, T8, respectively). In addition, a first-order Gauss-Markov process [8, 31] is used to simulate the ocean currents.

The parameters in the proposed controller are given as follows: $k=0.1$; $\gamma=1.2$; $c_1=0.2$; $d_1=1$; $k_1=0.5$, $k_2=0.5$, $k_3=1$, $k_4=1$, $k_5=10$; $h=0.05$, $\varepsilon=\mathrm{diag}(10, 10, 10, 10, 10, 10)$; $\Gamma_{\mathrm{WF}}=\Gamma_{\mathrm{WG}}=\mathrm{diag}(1, 1, 1, 1, 1, 1)$; $\Gamma_{\mathrm{VF}}=\Gamma_{\mathrm{VG}}=\mathrm{diag}(1, 1, 1, 1, 1, 1, 1, 1, 1, 1, 1, 1)$. The numbers of the input layer, recurrent layer, hidden layer and output layer of RNN are 6, 6, 12 and 6, respectively.

5.1.1 Trajectory Tracking Simulation

The proposed method is used to improve the tracking accuracy when the target trajectory has an abrupt change. Therefore, the mutation target trajectory is firstly considered in this paper. In addition, simulations with continuous desired trajectory are also considered.

(1) Tracking effect of the mutation target trajectory

The vertical DOF of AUV is easy to reflect the tracking effect of mutation target trajectory. In this section, the simulations will be conducted in 0.3 m/s ocean current environment and 0.5 m/s ocean current environment, respectively, and the 0.5 m/s is the maximum flow rate generated by the current-generating device in Section 5.2. In different ocean current environments, the target trajectories in vertical DOF are given as follows. During the experiments, the target trajectories are different, but the mutation amplitude of the trajectories is constant.

0.3 m/s ocean current environment:

$$Z=\begin{cases}0.9\,(\mathrm{m}), & t<40\ \mathrm{s},\\ 1.5\,(\mathrm{m}), & 40\ \mathrm{s}\le t<75\ \mathrm{s},\\ 1.0\,(\mathrm{m}), & 75\ \mathrm{s}\le t\le 100\ \mathrm{s}.\end{cases}$$

0.5 m/s ocean current environment:

$$Z=\begin{cases}0.6\,(\mathrm{m}), & t<40\ \mathrm{s},\\ 1.2\,(\mathrm{m}), & 40\ \mathrm{s}\le t<75\ \mathrm{s},\\ 0.7(\mathrm{m}), & 75\ \mathrm{s}\le t\le 100\ \mathrm{s}.\end{cases}$$

The simulation results of trajectory tracking control are shown in Figure 3.

In the evaluation of tracking performance, the following indexes are considered: average value of absolute tracking error (AVTE), mean square error of tracking error (MSETE), overshoot of tracking error (OTE) and adjustment time after target mutation (ATTM). The result can be seen in Table 2.

From Table 2, in the 0.3 m/s ocean current environment, compared with the Ref. [8], the evaluation index of AVTE, MSETE, OTE of proposed method are reduced by 29.06%, 7.05%, 65.72%, respectively. However, the AVTE, MSETE, OTE are reduced by 26.85%, 2.87%, 37.71%, respectively, in the 0.5 m/s ocean current environment. The simulation results show that the proposed method has a better transition characteristics and higher tracking accuracy.

In Table 2, in the 0.3 m/s and 0.5 m/s ocean current environment, compared with the Ref. [8], the ATTM of the proposed method is reduced by 48.84% and 42.86%, respectively. The result verified the quick convergence effect of the terminal sliding mode controller in the proposed method.

Further analysis, in different current environments, the simulation data of AVTE, MSETE, and OTE are roughly the same under the control of proposed method. However, the ATTM of 0.5 m/s ocean current environment

Table 1 Hydrodynamic parameters

	Surge	Lateral	Heave	Roll	Pitch	Yaw
Linear drag (N·s/m)	725	1240	825	3000	3000	1840
Quad. drag (N·s^2/m^2)	1000	525	400	100	100	72
Added mass (kg)	4380	9518	4268	5000	5000	5000

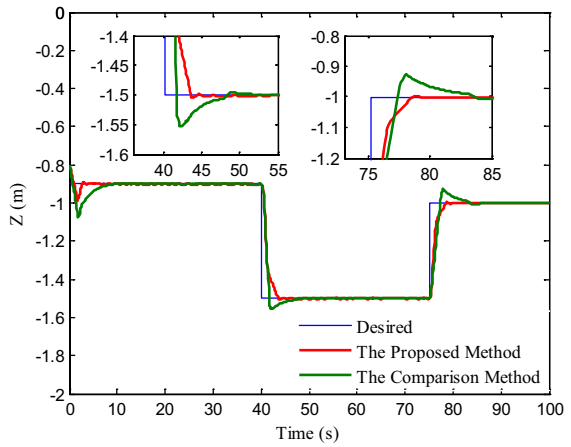

a Trajectory tracking of 0.3 m/s ocean current environment

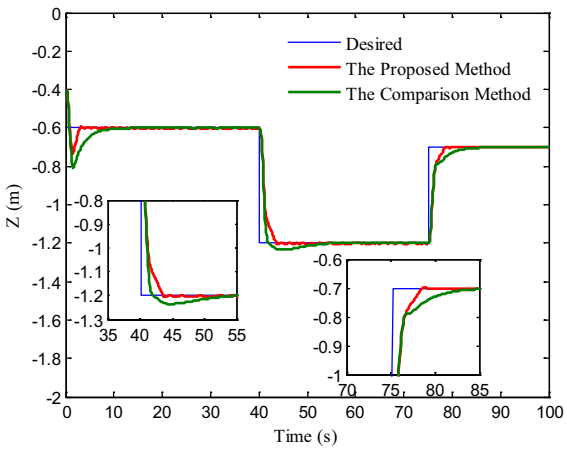

b Trajectory tracking of 0.5 m/s ocean current environment

Figure 3 Simulation curves of mutation trajectory tracking in different ocean current environments

is 5.6 s; compared with the ATTM (4.4 s) of 0.3 m/s, the data of 0.5 m/s increased by 21.43%.

In summary, under the control of the proposed method, the disturbances of ocean current have an influence on the adjustment time after target mutation (ATTM), and less influence on the trajectory tracking accuracy.

(2) Tracking effect for continuous target trajectory

The continuous target trajectory in Ref. [8] is used to simulation, and the target trajectory is written as

$$\begin{cases} x_d = 0.3t \text{ (m)} \\ y_d = 0.3t + 0.3\sin(0.2t) \text{ (m)} \\ z_d = -0.1t \text{ (m)} \end{cases}$$

$$\eta_d = [x_d, y_d, y_d, 0, 0, 0]$$

Table 2 Simulation data in different ocean current environment

	AVTE (m)	MSETE (m)	OTE (m)	ATTM (s)
0.3 m/s current				
The proposed method	0.0144	0.0659	0.0253	4.4
Ref. [8]	0.0203	0.0709	0.0738	8.6
Reduced by	29.06%	7.05%	65.72%	48.84 %
0.5 m/s current				
The proposed method	0.0158	0.0678	0.0218	5.6
Ref. [8]	0.0216	0.0698	0.035	9.8
Reduced by	26.85%	2.87%	37.71%	42.86%

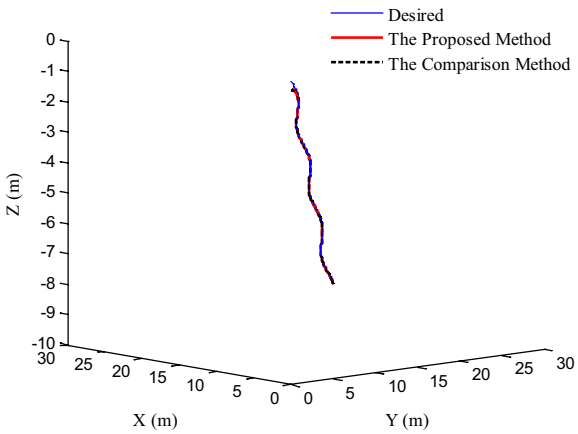

Figure 4 AUV continuous trajectory tracking in 0.3 m/s ocean current environment

The tracking experiments were conducted in the 0.3 m/s ocean current environments. And the simulation results are shown in Figure 4 and Figure 5. The details value about evaluation indexes are presented in Table 3.

From Table 3, compared with the Ref. [8], the AVTE is reduced [28.02%, 52.47%, 16.58%, 57.38%, 58.52%, 34.88%], respectively, in the direction of six DOF (X, Y, Z, Roll, Pitch, Yaw). And the MSETE is reduced [18.89%, 25.60%, −1.77%, 30.78%, 32.77%, 17.56%], respectively. The simulation results show the effectiveness of the proposed method in improving the tracking accuracy.

To test the trajectory tracking effect of the proposed method in different ocean current environments, the simulation in 0.5 m/s ocean current environment is conducted. The simulation data are shown in Table 4.

From Table 4, the trajectory tracking accuracy of the proposed method has been improved in 0.5 m/s ocean current environment, the simulation shows the effectiveness of the proposed method. Compared with the simulation data of Table 3 and Table 4 under the control of

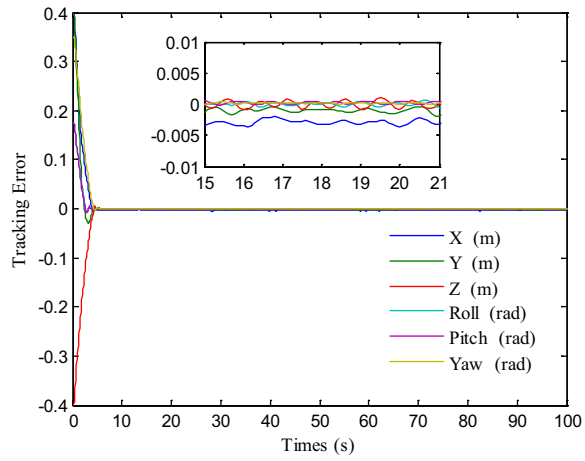

a Tracking error of the proposed method

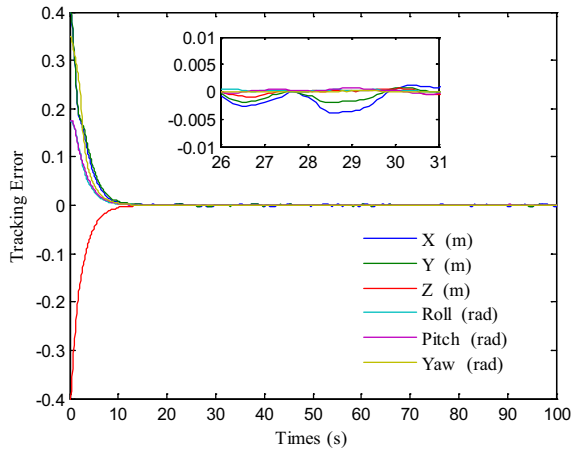

b Tracking error of Ref. [9]

Figure 5 Tracking error in 0.3 m/s ocean current environment

the proposed method, the tracking accuracy is approximately the same in 0.5 m/s and 0.3 m/s ocean current environments.

In summary, based on the simulation experiments, the proposed method has a better tracking accuracy and the convergence time of the tracking error is shorter than the Ref. [9] method. The results demonstrate the feasibility and effectiveness of the proposed method. Within 0.5 m/s, the data shows that different ocean current environments have less influence on the tracking accuracy under the control of the proposed method, but it has a certain influence on the adjustment time in mutation trajectory.

5.1.2 Contrast Simulation for Chattering-reduction Methods

For demonstrating the effectiveness of the proposed chattering-reduction methods, the compared simulation experiments are carried out with the fixed boundary layer in Ref. [18]. The tracking error of AUV, the control outputs of AUV thruster (control voltage) are shown in Figure 6.

In simulations, the mean square error of the control variables (MSECV), mean square error of the derivatives of control variables (MSEDCV) are used as the evaluation indexes of chattering amplitude and chattering frequency.

To verify the effectiveness of the proposed method, and does not affect the trajectory tracking accuracy, the evaluation index of MSETE is used. Hence, the relevant data in Figure 6 and Figure 7 are organized into Table 5.

From Table 5, compared with the Ref. [18], the MSECV of thruster are reduced [2.89%, −2.34%, 13.69%, 5.95%, 25.92%, 56.54%, 29.71%, 58.38%], respectively, based on the proposed method. The MSEDCV of thruster

Table 3 Simulation data in 0.3 m/s ocean current environment

	AVTE (m, m, m, rad, rad, rad)	MSETE (m, m, m, rad, rad, rad)
The proposed method	[0.0090, 0.0059, 0.0078, 0.0026, 0.0025, 0.0069]	[0.0402, 0.0366, 0.0438, 0.0167, 0.0166, 0.0397]
Ref. [8]	[0.0125, 0.0125, 0.0094, 0.0061, 0.0061, 0.0106]	[0.0496, 0.0491, 0.0430, 0.0242, 0.0247, 0.0482]
Reduced by	[28.02%, 52.47%, 16.58%, 57.38%, 58.52%, 34.88%]	[18.89%, 25.60%, −1.77%, 30.78%, 32.77%, 17.56%]

Table 4 Simulation data in 0.5 m/s ocean current environment

	AVTE (m, m, m, rad, rad, rad)	MSETE (m, m, m, rad, rad, rad)
The proposed method	[0.0117, 0.0076, 0.0082, 0.0031, 0.0029, 0.0071]	[0.0382, 0.0368, 0.0436, 0.0168, 0.0168, 0.0397]
Ref. [8]	[0.0123, 0.0121, 0.0094, 0.0063, 0.0052, 0.0098]	[0.0498, 0.0469, 0.0428, 0.0179, 0.0184, 0.0449]
Reduced by	[4.68%, 37.29%, 13.42%, 50.56%, 43.96%, 27.85%]	[23.33%, 21.55%, −1.84%, 6.31%, 8.65%, 11.69%]

are reduced [62.37%, 67.24%, 68.96%, 79.39%, 80.98%, 84.90%, 71.00%, 85.24%], respectively. The simulation results verify the effectiveness of the proposed method in reducing the chattering phenomenon.

Meanwhile, compared with the Ref. [18], the MSETE of the proposed chattering-reduction method is reduced [2.59%, 6.13%, 10.99%, 2.31%, 2.05%, 7.38%], based on the proposed method. The simulation results show that the proposed method can effectively reduce the sliding mode chattering, and the trajectory tracking accuracy of AUV can be increased a little.

5.2 Pool-Experiments of AUV Prototype

Furthermore, in order to demonstrate the feasibility and effectiveness of the adaptive backstepping terminal sliding mode control method based on RNN in actual experiments, the trajectory tracking of pool-experiments are conducted with self-developed UVIC-I AUV experimental prototype. Compared with the method in Ref. [8], the pool-experiments are carried out to verify the effectiveness of the proposed method in improving the tracking accuracy.

The shape of UVIC-I AUV experimental prototype is elliptical streamlined, shown in Figure 8(a). The length, width and height of AUV are 2.0 m, 0.6 m and 0.6 m. Its dry weight is 205 kg and slightly positively buoyant. There are eight thrusters, including two horizontal thrusters, two lateral thrusters and four vertical thrusters; the thruster configuration is shown in Figure 8(b). The sensor system includes depth, speed, attitude angle sensor, etc. The pool-experiments of UVIC-I AUV prototype in this paper are shown in Figure 8(c), the length,

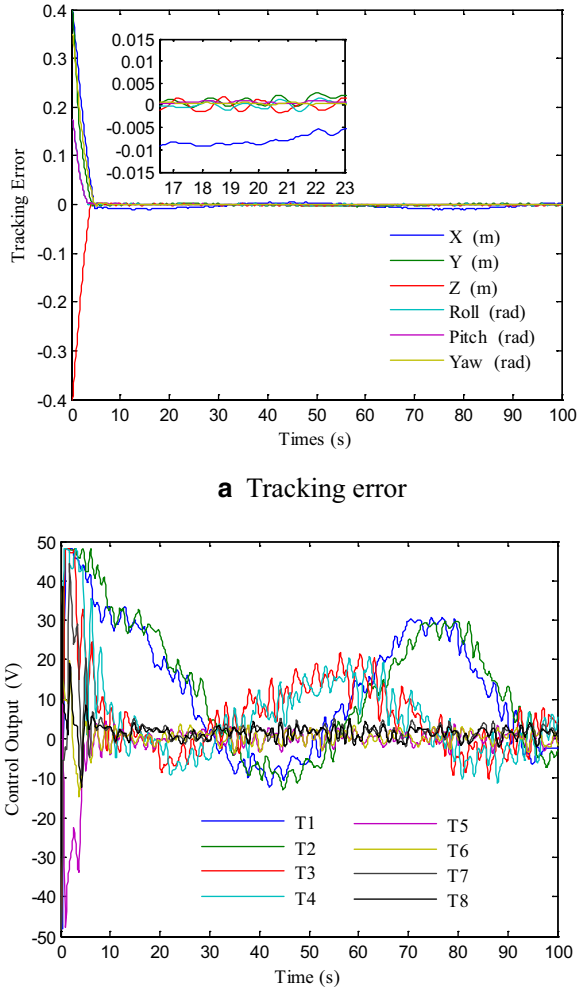

a Tracking error

b Control voltage for AUV thruster

Figure 6 Chattering-reduction effect of the proposed methods

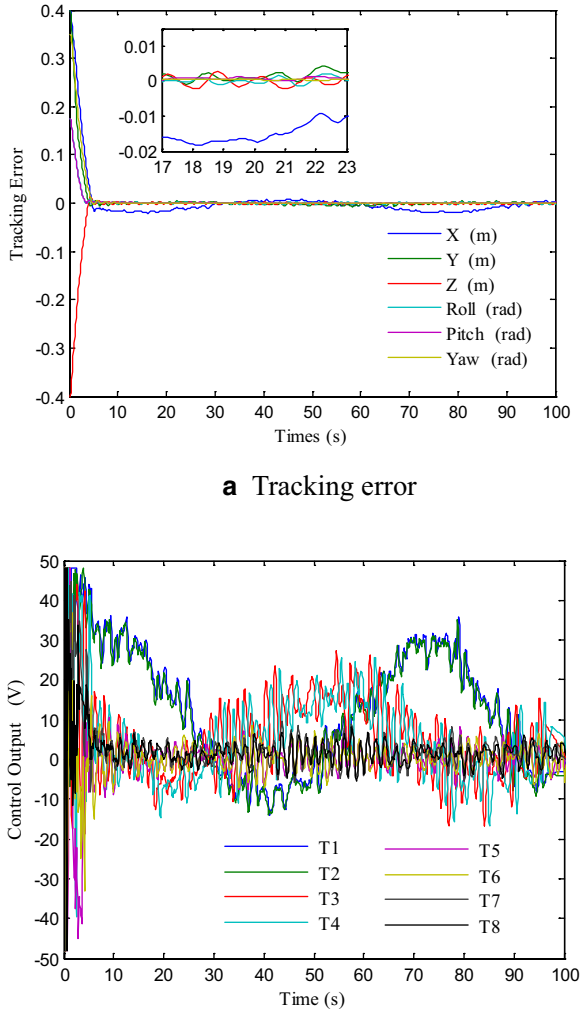

a Tracking error

b Control voltage for AUV thruster

Figure 7 Chattering-reduction effect of the Ref. [18]

Table 5 The chattering simulation experimental data

	MSECV (V)	MSEDCV (V)	MSETE (m, m, m, rad, rad, rad)
The proposed chattering-reduction method	[15.708, 16.424, 10.119, 11.139, 5.705, 2.682, 4.953, 2.184]	[1.047, 1.067, 1.194, 0.976, 0.998, 0.865, 0.871, 0.852]	[0.0489, 0.0404, 0.0436, 0.0178, 0.0175, 0.0403]
Ref. [19]	[16.177, 16.049, 11.725, 11.845, 7.702, 6.171, 7.047, 5.248]	[2.782, 3.256, 3.847, 4.735, 5.248, 5.729, 3.001, 5.771]	[0.0503, 0.0431, 0.0490, 0.0174, 0.0179, 0.0436]
Reduced by	[2.89%, −2.34%, 13.69%, 5.95%, 25.92%, 56.54%, 29.71%, 58.38%]	[62.37%, 67.24%, 68.96%, 79.39%, 80.98%, 84.90%, 71.00%, 85.24%]	[2.59%, 6.13%, 10.99%, 2.31%, 2.05%, 7.38%]

width and depth of the experiment pool are 50 m, 30 m and 10 m. When conducted the pool-experiments, the self-developed current-generating device is shown in Ref. [32], and the maximum velocity of irregular water current is 0.5 m/s.

(1) Tracking effect of the mutation target trajectory

Consistent with the simulation experiments, the trajectories tracking of pool-experiments were conducted in the ocean current environments of 0.3 m/s and 0.5 m/s. The desired trajectories are the same as the target trajectory in Section 5.1.1(1).

The pool-experimental results of the mutation target trajectory are shown in Figure 9. And the relevant data in Figure 9 is shown in Table 6.

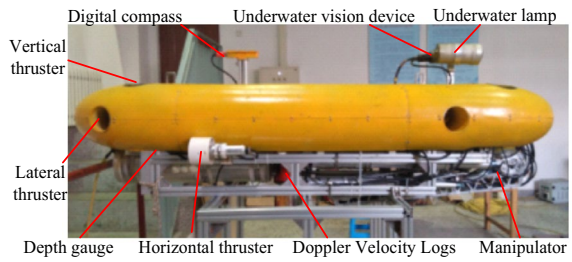

a Principle prototype

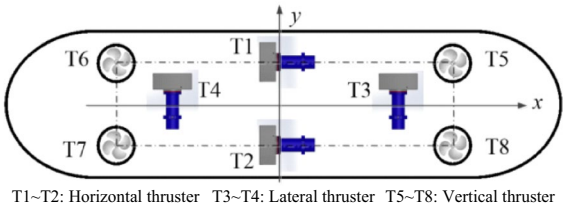

b Thruster configuration

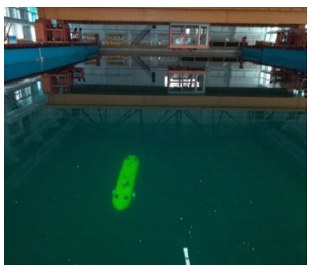

c Pool-experiments

Figure 8 UVIC-I AUV principle prototype

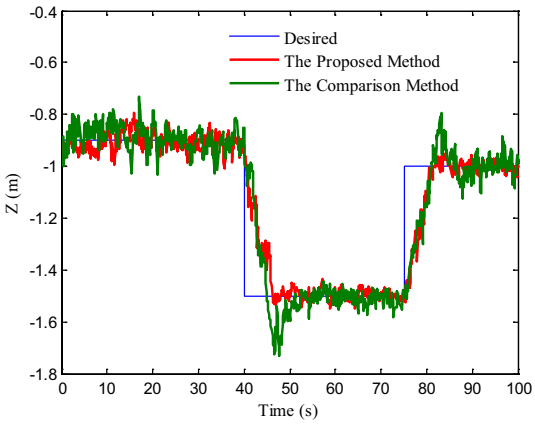

a Trajectory tracking of 0.3 m/s ocean current environment

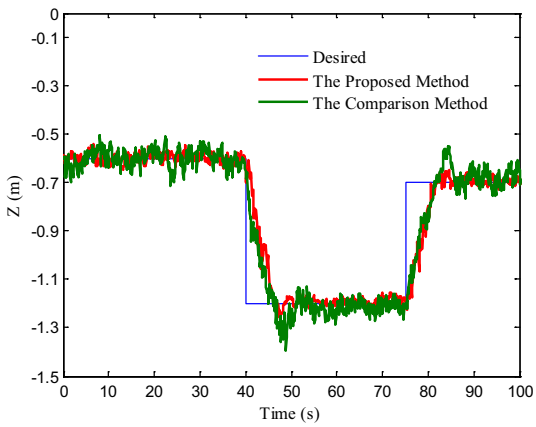

b Trajectory tracking of 0.5 m/s ocean current environment

Figure 9 Experimental curves in different ocean current environments

Table 6 Experimental data in different ocean current environments

	AVTE (m)	MSETE (m)	OTE (m)	ATTM (s)
0.3 m/s current				
The proposed method	0.0484	0.097	0.058	7.6
Ref. [8]	0.0680	0.119	0.207	10.9
Reduced by	28.82%	18.49%	71.98%	30.28%
0.5 m/s current				
The proposed method	0.0465	0.103	0.061	9.2
Ref. [8]	0.0616	0.115	0.194	11.7
Reduced by	24.51%	10.43%	68.56%	21.37%

From Table 6, compared with Ref. [8], the AVTE, MSETE, OTE, ATTM of the proposed method are reduced by 28.82%, 18.49%, 71.98%, 30.28%, respectively, in 0.3 m/s environment. However, in 0.5 m/s environment, AVTE, MSETE, OTE, ATTM are reduced by 24.51%, 10.43%, 68.56%, 21.37%, respectively. The results show that the proposed method has a better transition characteristics, higher tracking accuracy and quick convergence effect.

Consistent with the trend of simulation experiments, the experimental data of AVTE, MSETE, and OTE are approximately the same under the control of the proposed method. However, compared with 0.3 m/s ocean current environment, the ATTM of 0.5 m/s is increased by 17.39 %. The pool experimental conclusion is the same with the simulation experiments.

Comparing the experimental data of Table 2 and Table 6, there is a certain deviation between the simulation data and the pool experimental data. Compared with the simulation environments, the pool environments is more complicated, which is one of the reasons for the deviation. The simulation data is obtained through a mathematical model, and the pool data is measured by sensors, so the data deviation can also cause by the sensor measurement errors and model errors. However, the trend of pool-experimental data and simulation data is consistent, and the data are all in the same order of magnitude.

(2) Tracking effect for continuous target trajectory

In the pool-experiments, the tracking experiments of continuous target trajectory of AUV are carried out to test the tracking effect of the proposed method. Furthermore, in order to simplify the AUV pool-experiments, the target trajectory is the continuous trajectory of "vertical + heading" DOF.

The sine and cosine trajectories are chosen as the target trajectories of vertical and heading DOF. According to the velocity and acceleration of UVIC-I AUV, the proper trajectory frequency and amplitude are obtained. The continuous target trajectory of "vertical + heading" DOF is written as

$$z_d = 0.3t + 0.3\sin(0.2t) \quad \text{(m)}$$
$$\varphi_d = \frac{\pi}{2} + \frac{\pi}{4}\sin\left(\frac{2\pi}{70}t \times 0.2\right) \quad \text{(m)}$$
$$\eta_d = [0, 0, z_d, \varphi_d, 0, 0].$$

The tracking experiments of continuous target trajectory were carried out in 0.3 m/s environment. And the pool-experimental results are shown in Figure 10 and Figure 11. The relevant data are summarized in Table 7.

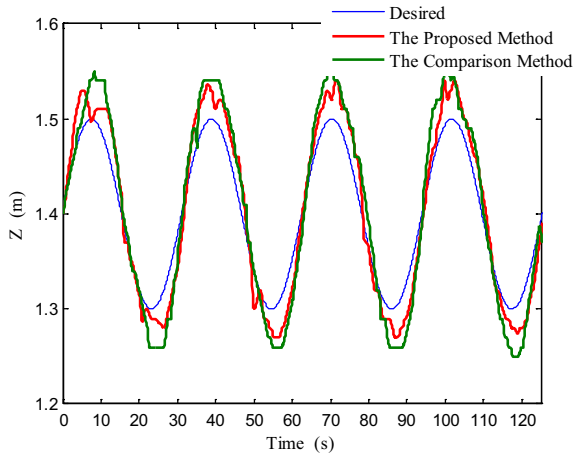

a Vertical DOF

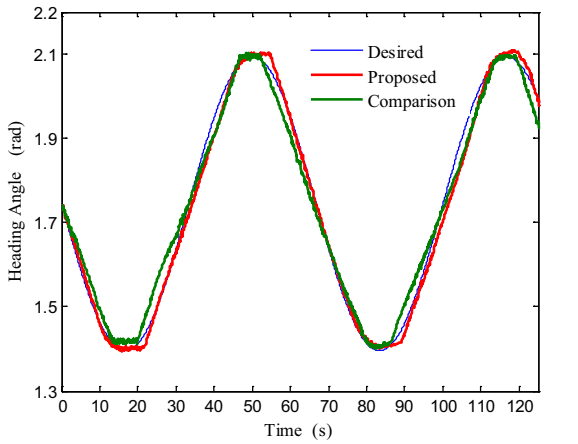

b Heading DOF

Figure 10 Continuous target trajectory tracking in 0.3 m/s ocean current environment

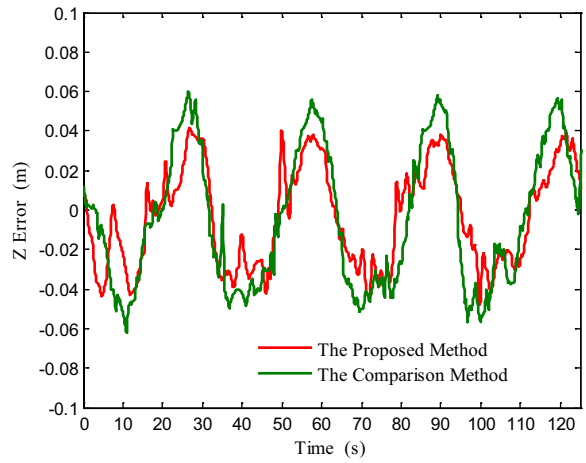

a Vertical DOF

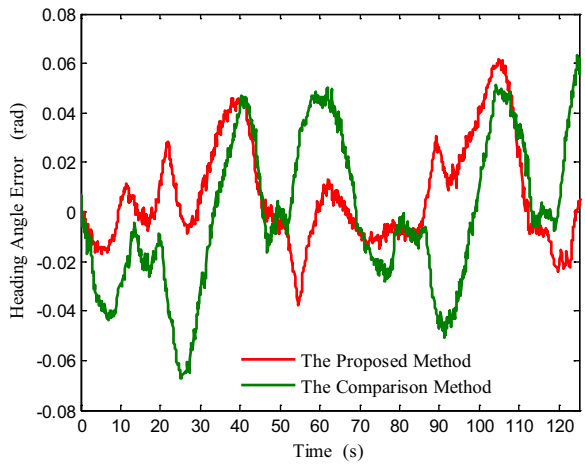

b Heading DOF

Figure 11 Tracking error in 0.3 m/s ocean current environment

From Table 7, compared with Ref. [8], in the direction of the vertical and heading, the AVTE and MSETE of the proposed method are reduced by [26.37%, 36.72%], [26.65%, 32.14%], respectively. The pool-experimental results show the effectiveness of the proposed method on continuous target trajectory tracking.

Table 7 Experimental data in 0.3 m/s ocean current environment

	AVTE (m, rad)	MSETE (m, rad)
The proposed method	[0.0229, 0.0162]	[0.0256, 0.0209]
Ref. [8]	[0.0311, 0.0256]	[0.0349, 0.0308]
Reduced by	[26.37%, 36.72%]	[26.65%, 32.14%]

Table 8 Experimental data in 0.5 m/s ocean current environment

	AVTE (m, rad)	MSETE (m, rad)
The proposed method	[0.0229, 0.0218]	[0.0280, 0.0251]
Ref. [8]	[0.0386, 0.0366]	[0.0441, 0.0394]
Reduced by	[40.61%, 40.53%]	[36.44%, 36.24%]

Consistent with the simulations experiments, the pool-experiments of continuous trajectory tracking is conducted in 0.5 m/s environment. The data are shown in Table 8.

From Table 8, compared with Ref. [8], the AVTE, MSETE of the proposed method were reduced by [40.61%, 40.53%] and [36.44%, 36.24%], respectively. And the experimental data shows the effectiveness of the proposed method. Compared with Table 7 and Table 8, under the control of the proposed method, the changes of AUV trajectory tracking accuracy is relatively small in the 0.5 m/s and 0.3 m/s environments.

In conclusion, based on the pool-experiments, the proposed method has a higher trajectory tracking accuracy for the trajectory tracking, and the tracking accuracy and convergence time are also better than the method in Ref. [9]. And the experimental data shows that the different ocean current environments have less influence on the tracking accuracy, but it has a certain influence on the adjustment time in mutation trajectory, the conclusion is consistent with the simulation experiments.

6 Conclusions

(1) In this paper, an adaptive backstepping terminal sliding mode control method based on RNN is proposed to solve the trajectory tracking problem of AUV under the influence of ocean current disturbance, dynamic modeling uncertainty, and thrust model errors. The SMU and ocean current disturbance are approximated online based on the RNN. And then through the backstepping terminal sliding mode controller, the neural network weight and control parameters are adjusted online. Based on Lyapunov theory and Barbalat's lemma, it is proved theoretically that the trajectory tracking error of AUV can quickly converge to zero in finite time. Simulations and pool-experimental results demonstrated that the proposed method has a superior trajectory tracking control accuracy and a better convergence time of trajectory tracking error. Under the control of the proposed method, the different flow velocities of the ocean current environment have less impact on trajectory tracking accuracy.

(2) Moreover, in order to solve the chattering problem of sliding mode control, a chattering-reduction method based on the sigmoid function is proposed. And according to the compared simulation results with traditional boundary layer method, it is indicated that the proposed method can effectively reduce the chattering phenomenon, and the experimental results show the effectiveness of the proposed method.

Authors' Contributions

M-JZ was in charge of the whole trial; CY wrote the manuscript; CY and FY assisted with sampling and laboratory analyses. All authors read and approved the final manuscript.

Authors' Information

Chao Yang, born in 1988, is currently a PhD candidate at *College of Mechanical and Electrical Engineering, Harbin Engineering University, China.* He received his bachelor degree and master degree in 2011 and 2013, from *Harbin Engineering University*, *China*. His research interests include underwater manipulator, AUV and intelligent control of manipulator.

Feng Yao, born in 1985, is currently a lecturer at *Harbin Engineering University, China.* His research interests include AUV, ROV and intelligent control.

Ming-Jun Zhang, born in 1963, is currently a professor at *Harbin Engineering University, China.* His research interests include mechanical engineering, ocean engineering and intelligent control of underwater vehicle.

Competing interests

The authors declare that they have no competing interests.

Funding

Supported by Basic Research Program of Ministry of Industry and Information Technology of China (Grant No. B2420133003) and National Natural Science Foundation of China (Grant Nos. 51779060, 51679054).

Publisher's Note

Received: 2 September 2017 Accepted: 7 December 2018
Published online: 26 December 2018

References

[1] Y R Xu, P C Li. The development trend of underwater vehicle. *Chinese Journal of Nature*, 2011, 33(3): 125-131. (in Chinese)
[2] C Z Pan, X Z Lai, S X Yang, et al. A bioinspired neural dynamics-based approach to tracking control of autonomous surface vehicles subject to unknown ocean currents. *Neural Computing & Applications*, 2015, 26(8): 1929-1938.
[3] O Hassanein, S G Anavatti, H Shim, T Ray. Model-based adaptive control system for autonomous underwater vehicles. *Ocean Engineering*, 2016, 127: 58-69.
[4] P S Londhe, M Santhakumar, B M Patre, et al. Task space control of an autonomous underwater vehicle manipulator system by robust single-input fuzzy logic control scheme. *IEEE Journal of Oceanic Engineering*, 2017, 42(1): 13-28.
[5] B Xu, S R Pandian, N Sakagami, et al. Neuro-fuzzy control of underwater vehicle-manipulator systems. *Journal of the Franklin Institute*, 2012, 349(3): 1125-1138.
[6] J C Yu, Q Li, A Q Zhang, et al. Neural network adaptive control for underwater vehicles. *Control Theory & Applications*, 2008, 25(1): 9-13. (in Chinese)
[7] A Bagheri, J J Moghaddam. Simulation and tracking control based on neural-network strategy and sliding-mode control for underwater remotely operated vehicle. *Neurocomputing*, 2009, 72(7-9): 1934-1950.
[8] Y J Wang, M J Zhang, P A Wilson, et al. Adaptive neural network-based backstepping fault tolerant control for underwater vehicles with thruster fault. *Ocean Engineering*, 2015, 110: 15-24.
[9] M J Zhang, Z Z Chu. Adaptive region tracking control for autonomous underwater vehicle. *Journal of Mechanical Engineering*, 2014, 50(19): 50-57. (in Chinese)
[10] JPJ Avila, DC Donha, JC Adamowski. Experimental model identification of open-frame underwater vehicles. *Ocean Engineering*, 2013, 60(2): 81-94.
[11] P Ridao, A Tiano, A El-Fakdi, et al. On the identification of nonlinear models of unmanned underwater vehicles. *Control Engineering Practice*, 2004, 12(12): 1483-1499.
[12] A Bagheri, T Karimi, N Amanifard. Tracking performance control of a cable communicated underwater vehicle using adaptive neural network controllers. *Applied Soft Computing*, 2010, 10(3): 908-918.
[13] M J Zhang, X Liu, B J Yin, et al. Adaptive terminal sliding mode based thruster fault tolerant control for underwater vehicle in time-varying ocean currents. *Journal of the Franklin Institute*, 2015, 352(11): 4935-4961.
[14] M J Zhang, Z Z Chu. Adaptive sliding mode control based on local recurrent neural networks for underwater robot. *Ocean Engineering*, 2012, 45(2): 56-62.
[15] Z Z Chu, D Q Zhu, G E Jan. Observer-based adaptive neural network control for a class of remotely operated vehicles. *Ocean Engineering*, 2016, 127: 82-89.
[16] Q Khan, R Akmeliawati. Neuro-adaptive dynamic integral sliding mode control design with output differentiation observer for uncertain higher order MIMO nonlinear systems. *Neurocomputing*, 2017, 226: 126-134.
[17] Z Z Chu, D Q Zhu, S X Yang, et al. Adaptive sliding mode control for depth trajectory tracking of remotely operated vehicle with thruster nonlinearity. *Journal of Navigation*, 2017, 70: 149-164.
[18] Y Wang, L Gu, M Gao, et al. Multivariable output feedback adaptive terminal sliding mode control for underwater vehicles. *Asian Journal of Control*, 2016, 18(1): 247-265.
[19] Y Feng, X Yu, Z Man. Non-singular terminal sliding mode control of rigid manipulators. *Automatica*, 2002, 38(12): 2159-2167.
[20] M D Tran, H J Kang. Adaptive terminal sliding mode control of uncertain robotic manipulators based on local approximation of a dynamic system. *Neurocomputing*, 2017, 228: 231-240.
[21] T Chatchanayuenyong, M Parnichkun. Neural network based-time optimal sliding mode control for an autonomous underwater robot. *Mechatronics*, 2006, 16(8): 471-478.
[22] S Yu, X Yu, B Shirinzadeh, et al. Continuous finite-time control for robotic manipulators with terminal sliding mode. *Automatica*, 2005, 41(11): 1957-1964.
[23] B Cong, X Liu, Z Chen. Backstepping based adaptive sliding mode control for spacecraft attitude maneuvers. *Aerospace Science & Technology*, 2013, 30(1): 1-7.
[24] G H Hardy, J E Littlewood, G Plya. *Inequalities*. Cambridge: University Press, Cambridge.
[25] Y Tang. Terminal sliding mode control for rigid robots. *Automatica*, 1998, 34(1): 51-56.
[26] V Nekoukar, A Erfanian. Adaptive fuzzy terminal sliding mode control for a class of MIMO uncertain nonlinear systems. *Fuzzy Sets & Systems*, 2011, 179(1): 34-49.
[27] J Yu, M Chen, C S Jiang. Adaptive sliding mode control for nonlinear uncertain systems based on disturbance observer. *Control Theory & Applications*, 2014, 31(8): 993-999. (in Chinese)
[28] W M Bessa, M S Dutra, E Kreuzer. Depth control of remotely operated underwater vehicles using an adaptive fuzzy sliding mode controller. *Robotics & Autonomous Systems*, 2008, 56(8): 670-677.
[29] S Soylu, B J Buckham, R P Podhorodeski. A chattering-free sliding-mode controller for underwater vehicles with fault-tolerant infinity-norm thrust allocation. *Ocean Engineering*, 2008, 35(16): 1647-1659.
[30] D Steinke. *Design and simulation of a Kalman filter for ROV navigation*. Canada: University of Victoria, 2006.
[31] T I Fossen. *Handbook of marine craft hydrodynamics and motion control*. Wiley, New York, 2011.
[32] W X Liu, Y J Wang, X Liu, et al. Weak thruster fault detection for AUV based on stochastic resonance and wavelet reconstruction. *Journal of Central South University*, 2016, 23(11): 2883-2895.